OPEN ACCESS
IOP Publishing
Plasma Physics and Controlled Fusion
Plasma Phys. Control. Fusion **65** (2023) 105001 (11pp)
https://doi.org/10.1088/1361-6587/aceeb2

Three-stage laser wakefield accelerator scheme for sub-Joule few-cycle laser pulses

Zsolt Lécz[1,*], Alexander Andreev[2], Daniel Papp[1], Christos Kamperidis[1] and Nasr A M Hafz[1,3]

[1] ELIALPS, ELI-HU Non-Profit Ltd, Wolfgang Sandner u. 3, Szeged, 6728, Hungary
[2] Max-Born Institute, Berlin, Germany
[3] Doctoral School of Physics, Faculty of Science and Informatics, University of Szeged, Dóm tér 9, Szeged 6720, Hungary

E-mail: zsolt.lecz@eli-alps.hu

Received 27 April 2023, revised 19 July 2023
Accepted for publication 9 August 2023
Published 22 August 2023

Abstract
Laser-driven electron acceleration in underdense plasma is a promising route towards the realization of reliable sources of relativistic electrons in the 0.1–1 GeV energy range. Generation of such electron bunches at high repetition rates is hindered by the limited energy per pulse, which inevitably results in very short pulse duration and tight focusing. Compressing the laser energy in time and space allows scientists to use higher plasma density to drive wakefieds, which in turn results in enhanced diffraction and dispersion of the broadband laser pulse. These features make difficult to control the acceleration in the plasma wave and to improve the beam quality. Here we propose a mm-long three-stage acceleration scheme, which allows for tunable injection and optimal acceleration of high-quality electron bunches. The full interaction length is modeled by 3D particle-in-cell simulations.

Supplementary material for this article is available online

Keywords: laser wakefield acceleration, few-cycle pulses, numerical modeling, laser guiding, GeV electron acceleration

(Some figures may appear in colour only in the online journal)

1. Introduction

Laser wakefield acceleration (LWFA) of electrons in underdense plasma has been developed to the point where the maximum electron energy is defined by the efficiency of the laser guiding [1, 2], since transverse confinement of the laser pulse is necessary to maintain the intensity. Gas-filled discharge capillary waveguides [3] are perfect solutions to extend the acceleration length up to the pump depletion length [4], which is proportional to the pulse duration and inversely proportional to the plasma density [5]. In a quasi-linear wakefield the accelerating field amplitude is proportional to the square root of density, thus by multiplying it with the depletion length we find an energy gain which is higher if longer pulses and more dilute plasma are used. The guiding is easier when the laser spot size is large, which allows for using capillaries with diameter much larger than the laser waist radius, thus avoiding the damage of the inner wall of the capillary. This technique seems highly feasible experimentally, but requires laser pulses

* Author to whom any correspondence should be addressed.

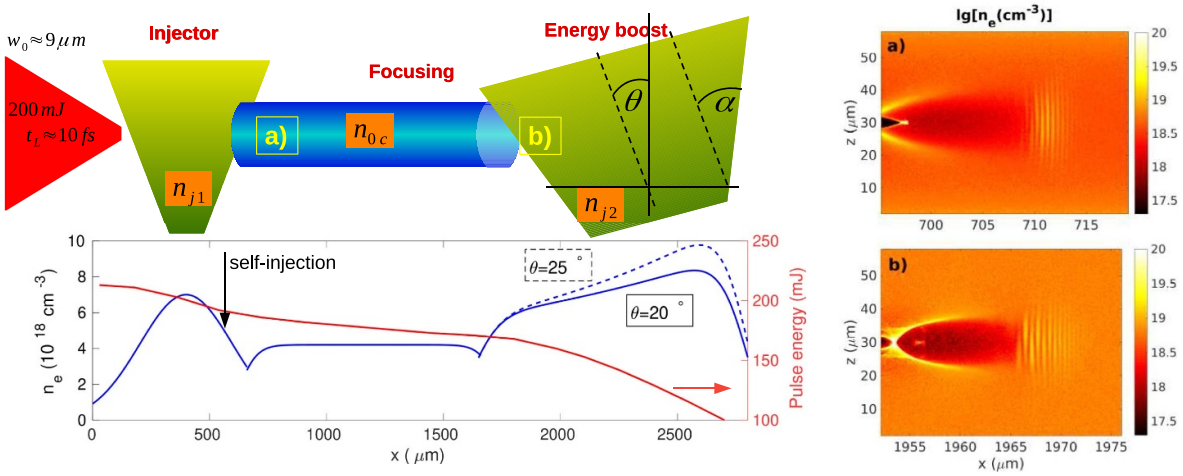

Figure 1. Sketch of the proposed experimental scheme. The laser pulse, with few hundred milli-Joule energy, is focused to the raising edge of a ∼300 μm wide gas jet with $n_{j1} = 7 \times 10^{18}$ cm^{-3}. Here the laser pulse triggers the self injection of ∼10 s of pC electron charge, which are accelerated to ∼70–100 MeV energy before entering the capillary stage (a), where $n_{0c} = 4.1 \times 10^{18}$ cm^{-3}. The spot size of the pulse is preserved in the first gas jet. The low-divergence laser pulse gets focused in the second stage, while it further accelerates the electrons. In the last stage (b) the laser pulse experiences significant plasma dispersion and for efficient acceleration the second gas jet with higher density ($n_{j2} = 6.7 \times 10^{18}$ cm^{-3}) and increasing density profile is applied.

with 10 s of Joules energy, reducing the practicality and the possible use in applications which require high repetition rate. Recently, some efforts have been put to manipulate the density profile in the waveguide [6] or to manufacture small diameter capillary with help of micro-machining [7], which allows for efficient guiding of tightly focused laser pulses as well.

From the view-point of applications [8–10], high average electron current and high sampling frequency are demanded, but current laser technology can provide laser pulses with very limited energy at such high repetition rates. For example, at ELI-ALPS the total energy in a single laser pulse will be on the order of 100 mJ compressed to less than 10 fs (a few laser cycles), leading to ∼10 TW power. Such an ultrashort laser pulse has to be focused to a spot radius of $w_0 \sim 10\,\mu$m in order to reach relativistic laser intensity ($>10^{18}$ W cm^{-2}) needed for driving a wakefield accelerator. Recent investigations have shown that the electron acceleration in a simple high density gas jet is very efficient, providing close to nC charge in a single shot with average energy around 200 MeV and with an exponential tail up to ∼300 MeV [11]. However, the energy spread is 100% and the beam quality is low, that should be improved by the careful control of the electron injection and pulse propagation inside the plasma.

Generally, a good quality LWFA requires two stages: electron injection and long acceleration [12, 13]. In the present work we incorporate an intermediate stage, which is necessary to re-focus the laser pulse after the injection stage. Thus, for the case of few-cycle laser pulses and in order to achieve high quality GeV-class electron beams, a three-stage acceleration scheme is proposed (see figure 1). It consists of a narrow gas jet, where the electron injection takes place; it is followed by a capillary discharge tube where the laser pulse is guided and re-focused within a millimeter length and finally the laser pulse enters a second gas jet, which is tilted relative to the vertical axis in order to compensate for the dephasing, developed due to plasma dispersion. We show that in the first stage it is possible to mitigate the pulse diffraction and to preserve the laser spot size, which is achieved by carefully choosing the focus (or focal plane) position relative to the position of the density peak in the gas jet. Up to now only several relevant experimental results have been published and they showed very different results, depending on the focusing optics or gas jet parameters [14–18]. The employment of a narrow gas filled capillary, as a discharge wave-guide, is reasonable since such devices have been proven to be stable at high repetition rates [19, 20]. Practically, the capillary discharge waveguide and the two gas jets can be embedded in one sapphire block, see [12], using laser micromachining technology. Furthermore, the total target system is only about 2 mm in length, allowing for a straightforward alignment and operation at high repetition rates.

The different behavior of ultra-short pulses was predicted theoretically in earlier works [21, 22], where it was shown that the critical power of self-focusing becomes much higher due to the density pile-up at the front of the pulse. The density modulation caused by the ponderomotive force can even cancel the relativistic self-focusing [23]. By approaching the few-cycle regime not only the broad spectrum leads to enhanced plasma dispersion effects, but also the large gradient in the refractive index causes strong spectral modulations and red shifting. In the opposite extreme case of very long pulses longitudinal self-phase modulation leads to periodic bunching of the laser envelope, which has been studied extensively [24–26]. Those long pulses can be effectively self-guided, but the wakefield generation is highly nonlinear and the electron acceleration is not controllable. For intermediate pulse lengths

(similar to the plasma wavelength) relativistic self-guiding has been observed experimentally [27–29], but for laser pulses 4–5 times longer than the pulse durations considered here. Therefore, in the case of few-cycle pulses one has to consider an external guiding structure, like a discharge capillary waveguide. In the next section it is shown that narrow capillaries are suitable to reverse the diffraction of the laser pulse and it is possible to extend the acceleration length by using a second gas jet.

The paper is structured in the following sections. We introduce an existing envelope guiding model [30] in section 2 to determine the plasma and laser parameters which allows for efficient self guiding in a tailored plasma profile consisting of three stages, shown in figure 1. In section 3 we present a 3D simulation where the initial conditions and parameters are based on the theoretical predictions of section 2. We shortly mention in section 4 that our setup can operate in the beam-driven regime as well, when the laser intensity is increased. Finally, the sensitivity of the proposed scheme is tested in section 5 with further simulations, where the initial setup is changed with respect to the optimal one, presented in section 3. We conclude our work in section 6.

2. Start-to-end modeling of the three-stage interaction

The shortness of a laser pulse is quite relative, because one can always find a plasma density which satisfies the condition $ct_L \approx \lambda_p\sqrt{\gamma}/2$, which ensures efficient wakefield (or bubble) formation. Here t_L is the laser pulse duration, $\gamma = \sqrt{1+a_0^2/2}$ is the average relativistic factor of the electrons, $a_0 = eE_L/(m_e\omega_0 c)$ is the normalized laser field amplitude, $\lambda_p = 2\pi c/\omega_p$ is the plasma wavelength and $\omega_p = (e^2 n_e/(m_e\epsilon_0))^{1/2}$. In the case of few-cycle pulses one can increase the plasma density, but the dephasing ruins the acceleration, because it scales strongly with electron density $\propto n_e^{3/2}$, while the accelerating field is proportional to $n_e^{1/2}$. In order to avoid strong wave-breaking and beam loading one has to consider lower plasma densities ($\omega_p < \pi\sqrt{\gamma}/t_L$), where the acceleration is limited by the pump depletion with a characteristic length: $L_d = ct_L n_c/n_e$, where $n_c = \omega_0^2\epsilon_0 e^2/m_e$ is the critical density. In this regime the pulse duration is not matched to the cavity length, but matching the laser spot radius (w_0) is still possible [31]: $w_0 \approx \lambda_p\sqrt{\gamma}/2 > ct_L$.

The relatively tight focusing brings a new limiting factor in the acceleration scheme, which is the diffraction length, or Rayleigh length ($L_R = \pi w_0^2/\lambda_0$, where λ_0 is the laser wavelength). It is obvious that guiding is meaningful when $L_d > 2L_R$, which leads to a threshold pulse duration (assuming matched spot size): $N > \gamma\pi/2$, where $N = ct_L/\lambda_0$ is the number of laser cycles within the FWHM of the intensity envelope. In the case of high intensity pulses ($a_0 > 1$) it is exactly the few-cycle regime and this is the typical pulse length ($N \leqslant \gamma\pi/2$) that we consider in our work. We present additional simulations in the supplementary material, which highlights the difference between the propagation of few-cycle and longer pulses in underdense plasma.

In this work for particle-in-cell modeling we use EPOCH [32]. In the case of a full-scale three-dimensional simulation the transverse dimensions of the simulation domain is strongly limited due to computational requirements. Therefore, the width of the simulation box is 60 μm, while the length in the x direction is 24 μm. The grid size is 40 nm in the longitudinal and 120 nm in the lateral directions, thus the space in the moving window is resolved by $600\times500\times500$ grid points. In each grid cells four electron macroparticles are initialized. The field solver is of 4th order and the time step is 30% of the Courant time step, which ensures negligible dispersion error over the full propagation distance. This is particularly important in the case of few cycle pulses, where the spectrum is relatively broad and the phase velocity should not be influenced by the grid dispersion.

The plasma density in the first stage was chosen such that the matching condition is fulfilled: $w_0 \approx \lambda_p\sqrt{\gamma}/2$. It means that for $w_0 = 9\,\mu$m the required average electron density is $n_e \approx 6\times10^{18}\,\mathrm{cm}^{-3}$. For a pulse duration of about 12 fs and wavelength of $\lambda_0 = 800$ nm the theoretical depletion length is around 1.5 mm at this plasma density. In the capillary the density is lower, therefore the laser pulse loses significant energy only in the first and third stages of the interaction (see figure 1). External electron injection is not considered in the modeling, but later we show that self-injection happens naturally in the rear side of the gas jet, in the density down-ramp, similarly to the case presented in [12]. The first gas jet has an important role also in the guiding of the pulse, because for an optimal focus position the laser spot size remains almost constant while it propagates through the gas jet.

In the following we show that, if the longitudinal evolution of the pulse shape is neglected, a laser pulse can be guided more safely in a capillary when $a_0 \gg 1$. We start with the envelope equation for the laser spot radius [33]:

$$\frac{\partial^2\rho}{\partial x^2} = \frac{4}{k_0^2 w_0^4\rho^3}\left(1 - \frac{a_0^2}{32}k_p^2 w_0^2 - \frac{\Delta n}{\Delta n_c}\rho^4\right), \qquad (1)$$

where $\rho = w/w_0$ is the spot radius normalized to the initial waist size (w_0), k_0 and k_p are the laser and plasma wave numbers, respectively. Here the channel depth ($\Delta n = n_p(w_0) - n_0$) is calculated from the realistic density profile [34, 35]: $n_p(r) \approx n_0 + (1/3)n_0 r^2/R_c^2$, which is valid only close to the axis: $r < R_c/2$ (see supplementary material). The critical channel depth, which is optimal for guiding, is given as $\Delta n_c = (\pi r_e w_0^2)^{-1}$, where $r_e = e^2/(4\pi\epsilon_0 m_e c^2)$ is the classical electron radius. Theoretically, ideal guiding is achieved when the right hand side of equation (1) is zero and $\rho = 1$. This leads to a quadratic equation for the matched initial laser spot radius ($w_0 = w_m$):

$$\frac{w_m^4}{12R_c^2} + \frac{w_m^2 a_0^2}{32} - \frac{1}{k_p^2} = 0. \qquad (2)$$

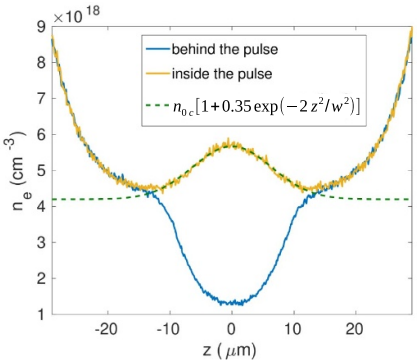

Figure 2. Radial density profiles in a discharge capillary when the laser pulse is also present. Behind the laser pulse (averaged between $x = 703$–709 μm in figure 1(a)) a deep quasi-parabolic profile appears due to electron cavitation, while inside the pulse (averaged between $x = 709$–713 μm in figure 1(a)) a density hump is observable, due to the longitudinal ponderomotive force. The center of the laser pulse is at $x = 711$ μm.

One can easily verify that in the limit $a_0 \to 0$ the well-known non-relativistic matched spot size is recovered: $w_{m,nr}^4 = R_c^2/(\Delta n_{ch} \pi r_e)$, where $\Delta n_{ch} = n_0/3$ in our case. After analyzing the solution of equation (2) we found that the guided laser spot size can be as small as $w_m < R_c/3$ if $k_p R_c a_0^2 \gg 32$, which is easily fulfilled for $a_0 > 2$. Smaller laser spot means lower intensity at the capillary walls, thus less damage is expected.

The estimations made above have limited validity when we take into account the longitudinal evolution of the laser pulse. Plasma dispersion (which leads to pulse elongation) and redshifting [36] can cause significant change in the peak intensity on a longer time scale. All these spectral changes are proportional to a_0^2, therefore we cannot increase the laser intensity arbitrarily. On the other hand, the ponderomotive repulsion changes the density profile of electrons, witnessed by the laser pulse, which we express as:

$$n_e(r) \approx n_b(r) + \delta n \exp(-2r^2/w^2), \tag{3}$$

where n_b is the background (unperturbed) plasma density, which can also depend on radius in a capillary, for instance. The generated density modulation is proportional to the radial profile of the laser intensity [23] as it is confirmed in figure 2. In our simulations for such a few-cycle pulse we observed $\delta n \approx 0.3 n_b$ up to $0.5 n_b$ averaged along the laser propagation axis, but it depends on the pulse duration as well. For 12 fs pulse duration we found good agreement with the fitting function using $\delta n = 0.35 n_b$. In the case of long pulses, in the blow-out regime, the density has a minimum along the axis ($r = 0$) and $\delta n < 0$ [37–39], which is also visible behind the laser pulse in figure 2. If the pulse is longer its central part is guided in this density modulation, i.e. in the self-generated channel. In principle the head of a laser pulse (the first few cycles) always experiences an increased density with quasi-Gaussian radial profile, which causes enhanced diffraction in this portion of the pulse. In the case of few cycle pulse the whole pulse experiences this modulated refractive index, which can be compensated only by external guiding, which is provided by a discharge capillary in our case.

Considering the self-consistent plasma density modulation, it can be easily recognized that in reality perfect guiding does not exist, only at low intensity [40]: $a_0 < 1$. At high intensity the pulse envelope oscillates, higher order Laguerre modes can appear [36, 41], and it can strongly interact with the capillary wall. Recently a regenerative discharge waveguide was proposed which can be used to mitigate the problem of radiation damage [42]. However, if a short capillary is considered, where the time is not enough for longitudinal pulse evolution, then a simplified model is reliable and it is shown that the condition $w < R_c/2$ can be maintained. In the case of tight focusing, we have to take into account δn and the exact density profile (n_b), which closely reproduces the density profile observed in relevant capillary discharges (see supplementary material) [34]:

$$n_b(\rho)/n_0 = 1 - 0.119\rho^2 + 2.3\rho^3 - 3.056\rho^4 + 2.05\rho^6. \tag{4}$$

The advantage of equation (4) is its easy implementation in particle-in-cell codes for the initialization of the density profile.

The propagation of a Gaussian laser pulse in underdense plasma can be well described with the model presented in [30] if we assume that the intensity profile remains Gaussian over the entire propagation distance. In the supplementary material we show that the Laguerre modes exist only for a short time in the capillary and those are negligible when the pulse intensity is increased. This model incorporates the time dependence of the laser spot radius and the relativistic effects are also included ($\gamma > 1$). The envelope equation describing the evolution of the laser spot size in the paraxial approximation is written in the following form:

$$\frac{d^2 w}{dx^2} = -2\frac{K(w,x)}{w} + \frac{4}{k_0^2 w^3}, \tag{5}$$

where $K(w,x)$ is a radially averaged quantity which incorporates the plasma response in a more general way. It is evaluated numerically by performing the following integral:

$$K(w,x) = -\left[\frac{\omega_{p0}(x)}{ck_0}\right]^2 \int_0^{R_c} \frac{4r}{w^2}(1-s)e^{-s}\frac{n_e(r)}{n_0} \times \left(1 + \frac{e^{-s}}{2W^2}\right)^{-1/2} dr, \tag{6}$$

where $s = 2r^2/w^2$, $W = w/(w_0 a_0)$ and $n_0 = n_e(0)$ is the density along the laser propagation axis. The advantage of this method is that we can include arbitrary radial dependence of the plasma density and it is possible to model the pulse propagation in a plasma channel or in a density ramp. In the simplified model of equation (1) a parabolic density profile is assumed, while our function (equation (4)) is more accurate over the whole capillary diameter.

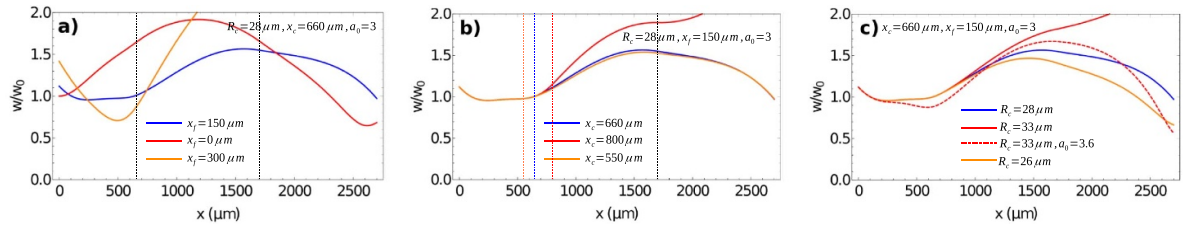

Figure 3. Modeling the influence of different parameters: (a) the focus position, (b) position of the capillary and (c) radius of the capillary. In (c) the effect of higher laser intensity is also shown. In all cases $\delta_n = 0.35 n_b$, the laser waist radius is $w_0 = 9\,\mu$m and the plasma density profile is the same as in figure 1. The vertical dashed lines show the borders between consecutive stages.

Now, by using equations (4)–(6) it is possible to model the first two stages of the scheme presented in figure 1. In the third stage the energy depletion is not negligible, therefore the predictions of the model are only qualitatively valid. The longitudinal density profile of the first gas jet is Gaussian described with $n_e = n_{j1}\exp(-(x-x_{01})^2/\sigma_{j1}^2)$, where $n_{j1} = 7.5\times10^{18}\,\mathrm{cm}^{-3}$, $\sigma_{j1} = 280\,\mu$m and $x_{01} = 400\,\mu$m. The capillary starts at $x = 660\,\mu$m and its length is $1040\,\mu$m with lower density on axis: $n_0 = 4.2\times10^{18}\,\mathrm{cm}^{-3}$. The lower density is needed for phase matching, i.e. the length of the wakefield ($\approx\sqrt{\gamma}2\pi c/\omega_p$) inside the capillary should be equal to the wavelength at the position of electron injection inside the gas jet (see figure 1).

The most important quantity in the proposed scheme is the position of the laser focus. In order to model focusing we define the laser spot size, $w = w_0\sqrt{1+(x-x_f)^2/L_R^2}$, where x_f is the focus position, and its derivative (dw/dx) as initial conditions in equation (5). The density up-ramp strongly influences the pulse propagation, because the scale length of the density variation has a similar dimension as the Rayleigh length of the focused laser pulse. Transforming equation (5) into a form similar to equation (1) one gets:

$$\frac{\partial^2\rho}{\partial x^2} = \frac{4}{k_0^2 w^4 \rho^3}\left(1-\frac{1}{2}k_0^2 w^2 K\right), \tag{7}$$

From equation (6) one can easily observe that $K\propto(k_0 w)^{-2}$, therefore the right hand side of equation (7) is close to zero when the x-dependence is eliminated from the integral, which requires a longitudinal density profile (close to $r=0$): $n_e(x)\propto\sqrt{1+2a_0^2/(1+(x-x_f)^2/L_R^2)}$. Since this function is similar to a Gaussian for $x-x_f<L_R$, the pulse diffraction is suppressed inside the gas jet and the scale length of the density gradient should be close to the Rayleigh length of the laser pulse (for more details see the supplementary material). This effect is shown in figure 3(a), where the laser spot radius remains almost constant if the focus position is $x_{01}-x_f = 250\,\mu$m ($\approx 0.83 L_R$) behind the center of the gas jet.

The position of the capillary entrance is also important, obviously it should be close enough to the gas jet in order to avoid a large laser spot radius entering the waveguide. In figure 3(b) one can see that this position should be at $x<700\,\mu$m, which means less than $300\,\mu$m ($\approx L_R$) from the center of the gas jet. Another important parameter is the radius of the capillary playing an important role in the re-focusing of the laser pulse. According to figure 3(c) the optimum value is around $R_c = 28\,\mu$m, a larger radius leads to more loose focusing and the laser spot expands significantly even if the laser intensity is increased (red dashed line in figure 3(c)). A smaller capillary radius results in stronger focusing, but the condition $R_c \gg w_0$ is more difficult to fulfill. We present more extensive modeling of the pulse propagation in capillaries in the supplementary material, where we show the upper limits of R_c that can be used to focus a given laser pulse.

At the exit side of the capillary the laser pulse acquires a negative divergence and gets focused again, therefore one can use it to drive a strong wakefield again. For this purpose a second gas jet is placed behind the capillary, where the plasma density can be higher, because the laser intensity increases, due to self-focusing. For keeping the electron bunch at the same accelerating phase of the wakefield the group velocity of the laser pulse has to be compensated by the shortening of the plasma wavelength [43]. Mathematically it can be formulated as $d\lambda_p/dt = v_g - c - v_d$, where $v_d \ll c$ is the backward velocity of the peak intensity of the pulse in a frame moving with c. By using the expression $v_g = c\sqrt{1-(\omega_p^2/\gamma)/\omega_0^2}$ we obtain the following dimensionless equation:

$$\frac{d}{d\xi}\left(\sqrt{\frac{n_c a_0}{n_b}}\right) = \sqrt{1-\frac{n_b+\delta n}{n_c a_0}} - 1 - \frac{v_d}{c}, \tag{8}$$

where $\xi = x/\lambda_0$. During the propagation in the plasma the pulse acquires a positive chirp, which results in a back-shift of the peak intensity, which is the origin of v_d. This effect is clearly visible in simulations shown by figure 6. For simplicity we assume that the laser field amplitude is constant ($a_0 = 2$), which is justified by the fact that the increase of intensity due to self-focusing is almost compensated by the energy depletion, therefore the field amplitude can be considered constant.

The desired density up-ramp is achieved by a simple method: the axis of the vertical gas jet is tilted by $\theta\approx 20°$. Due to the transverse expansion of the gas flow the density decreases along the vertical axis as $n_e\sim[1+(h/R_N)\tan\alpha]^{-2}$, where R_N is the radius of the nozzle, h is the height measured from the tip of the nozzle and α is the half opening angle (radial expansion) of the gas flow. By applying

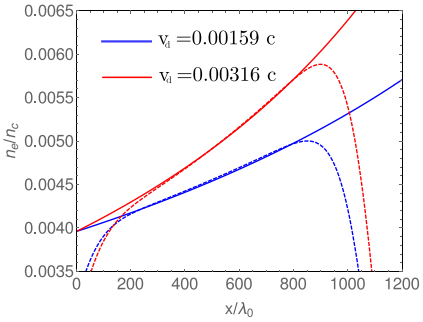

Figure 4. Full lines: solution of equation (8) for two values of v_d. Dashed lines: represent the density profile given by equation (9) for two tilting angles: $\theta = 14^\circ$ (blue) and $\theta = 22.5^\circ$ (red). Here $\delta n/n_b = 0.3$, $\alpha = 20^\circ$ and $R_N = 600\lambda_0$. Here $x = 0$ means the end of the capillary.

coordinate transformation the density profile along the laser axis ($x-$direction) has the form:

$$n_e(x) = n_{j2}\frac{\exp[-(x-x_{02})^p/(R_N)^p]}{[1-x\tan\alpha\tan\theta/R_N]^2}, \qquad (9)$$

where θ is the angle between the axis of the gas jet and the vertical coordinate and x_{02} is the position of the center of the nozzle. For the second nozzle we consider a flat-top density profile, therefore in our simulations a super Gaussian function is used with $p = 8$. It is remarkable that one can find a θ angle which provides a density up-ramp that matches perfectly with the desired phase-locking density ramp, which is seen in figure 4. The effect of chirp evolution (v_d) is demonstrated in figure 4, where the full lines show the theoretical density profiles needed for perfect phase locking (solution of equation (8)) and the dashed lines represent the density given by equation (9). For a larger v_d (shorter pulse, stronger dispersion) one needs a larger tilt angle (θ) to make the density profile steeper. The value of v_d is not known exactly, but in experiments the θ angle can be easily adjusted until optimal acceleration is achieved.

3. Proof-of-principle simulations and comparison with a two-stage scheme

First we present the reference case, when the beam loading of the wakefield is negligible and high quality, high energy electron bunch is produced. The physical parameters of the system are the same as in section 2: laser spot size is $w_0 = 9\,\mu$m, contains 220 mJ energy compressed to 12 fs (FWHM) duration and it is focused at $x_f = 150\,\mu$m. The wavelength is $\lambda_0 = 800$ nm. The normalized laser field amplitude is $a_0 = 2.75$. The radius of the capillary is $R_c = 28\,\mu$m. After the laser pulse crosses the center of the gas jet it propagates in a density down-ramp, thus the plasma wavelength, and the length of the wakefield, increases. This is shown by drawing the axial density distribution in figure 5, where $v_w = c\sqrt{1-1.5n_0/n_c}$ is the average group velocity of the laser pulse and this is the velocity

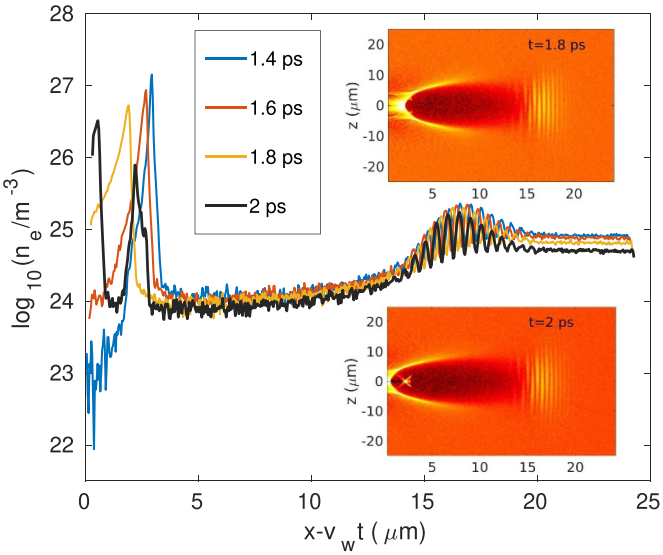

Figure 5. Longitudinal density profiles, along the laser propagation axis at different time instances. The insets show the transverse cross-section of the electron density distribution, which shows that the electron injection happens somewhere around $x = 570\,\mu$m ($t = 1.9$ ps). The label of the horizontal axis is the same as in the main picture.

of the moving window. The location of the density peaks in the back of the bubble is shifted backward, which means a decreasing phase velocity of the wakefield. At this stage the electron's velocity inside the density peak can easily become higher than the phase velocity of the bubble, which is exactly the condition for self-injection.

The wakefield evolution is presented in figure 6 together with the longitudinal phase-space distribution of the injected bunch. The first picture corresponds to the time instance right after the laser pulse enters the capillary. At this stage the electrons manifest a positive energy chirp and the tail of the bunch modifies the wakefield significantly (see figure 6(a)). A significant amount of low energy electrons are lost during the propagation through the capillary. It happens because the focusing field is weaker in the low density plasma and the electrons with large divergence can escape radially. The laser field amplitude at the beginning of the capillary is $\approx 8.8\,\mathrm{TV\,m^{-1}}$, which corresponds to $a_0 = 2.2$. Taking into account 10% energy loss in the first stage, the laser spot size is found to be almost unchanged. Inside of the capillary a linear wakefield is generated which increases the positive energy chirp, but at the same time it accelerates further the electrons (see figure 6(b)).

The capillary ends at $x = 1700\,\mu$m and it is followed by the second gas jet, which is tilted by $\theta = 22.5^\circ$, thus the laser pulse experiences a density profile shown by the red dashed curve in figure 4 and $n_{j2} = 0.004n_c = 1.6n_0$. The center of this gas jet is at $x_{02} = 2200\,\mu$m. At this stage the electron bunch is accelerated in a positive slope of the field, which results in the energy dechirping observed in figures 6(c) and (d). Note that the E_x field amplitude in the gas jet is about ten times higher

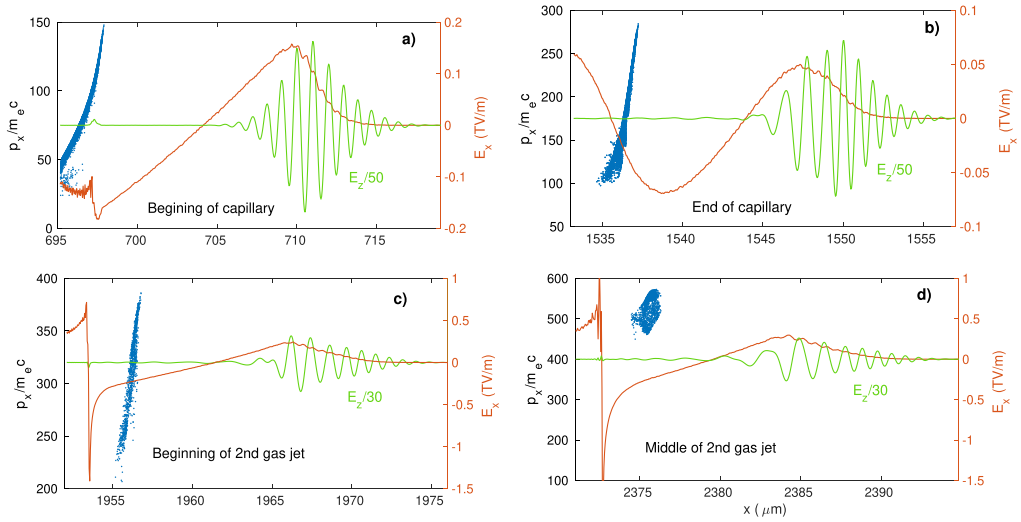

Figure 6. Phase-space distribution of electrons (blue dots) and accelerating electric field profiles (red lines) at different time instances: 2.4 ps (a), 5.2 ps (b), 6.6 ps (c) and 8 ps (d). The laser field is also shown by green that uses the scale of the right vertical axis.

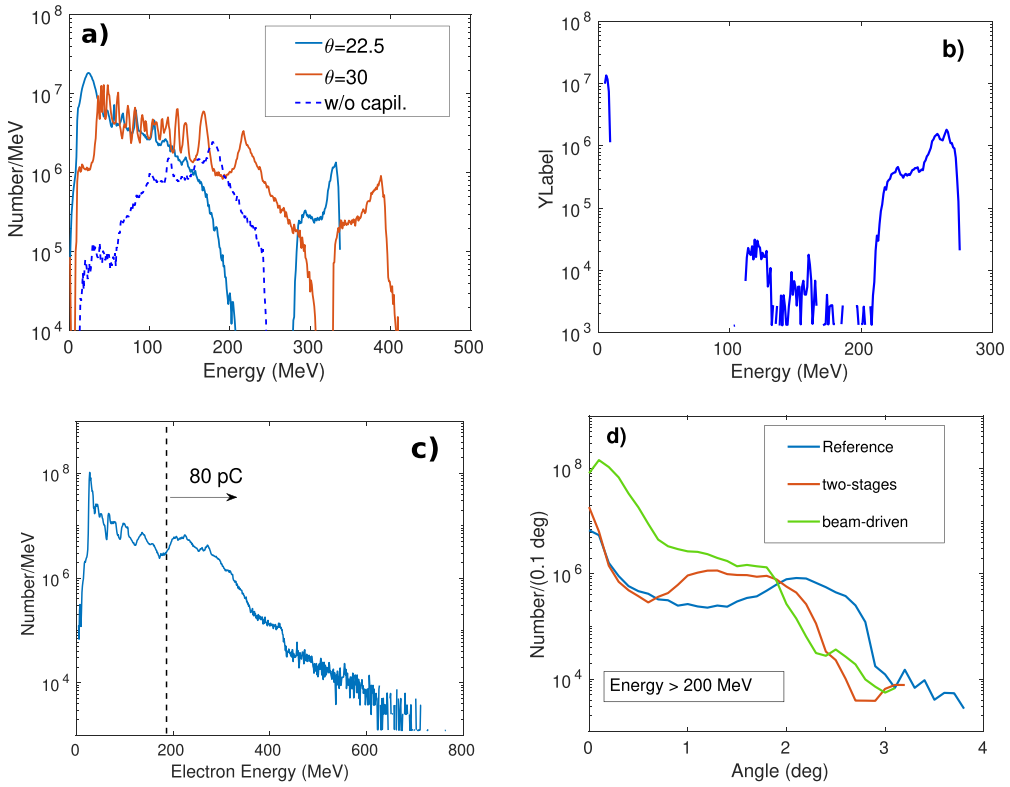

Figure 7. (a) Energy spectra of electrons for two values of θ upon exiting the second gas jet. The blue curve correspond to the case presented in figure 6. The dashed line shows the spectrum obtained in a scenario where no capillary was used (see figure 8). (b) Energy spectrum obtained by using a longer capillary (2.4 mm long), without using a second gas jet. (c) Final energy spectrum of electrons when the laser pulse energy was increased by 20%. The injected charge, obtained by integrating the spectrum above the vertical dashed line, is 80 pC, which is ten times more than with the original pulse energy. All other parameters are the same as in the case of the red curve in (a). (d) Comparison of electron angular distributions in the three cases presented in (a)–(c).

than in the capillary. From the middle of this gas jet the laser pulse acquires a positive frequency chirp and it gets elongated. The red-shifted laser pulse is slower than the electrons and it can interact with the electron bunch, therefore the width of the second gas jet is limited by this effect. We have tested a larger angle as well ($\theta = 30^\circ$) and the final energy spectra are compared in figure 7(a). In both cases secondary injection occurs near the rear side of the gas jet, where the plasma dispersion is very strong and the phase velocity of the wakefield gets reduced significantly. One can avoid this abundant self-injection by choosing shorter (narrower) gas jet or by decreasing the tilt angle.

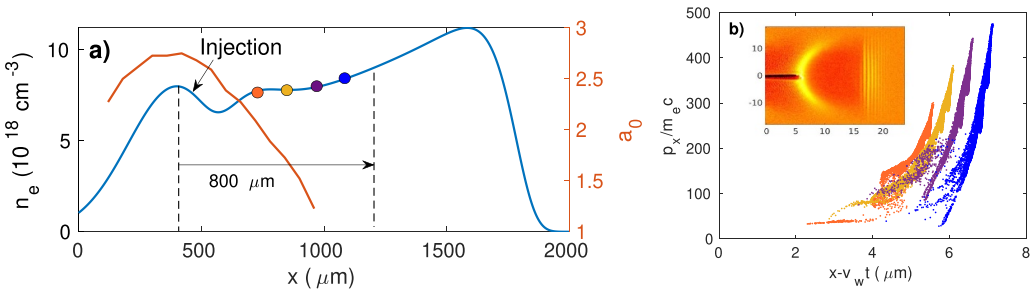

Figure 8. (a) Density profile of the plasma after removing the capillary and moving the two gas jets closer. The density in both targets has been increased by 10% in order to trigger the electron injection a little earlier (close to the first density peak). All other parameters are the same as before and $\theta = 22.5°$. (b) Phase-space evolution of the injected electrons at the positions indicated by the colored circles in (a). The inset shows the density distribution of electrons (same color scale as before) at the instance of the purple (third) point in (a). The label of the horizontal axis is the same as in the main picture.

The large energy gain, observed in the simulations, is a consequence of the second gas jet, where electron de-phasing is suppressed and strong wakefield is generated. The necessity of this third stage is proven by performing another simulation, where the second gas jet is missing and a longer capillary is used, which is exactly the setup considered in [12]. In this situation the energy spread is similar, but the central energy in the bunch is lower, which is shown in figure 7(b). The small energy spread is reached by phase-space rotation, which is presented in the supplementary material. In section 2 it was mentioned that a higher laser intensity enhances the guiding efficiency inside the capillary due to relativistic mass increase of plasma electrons. The better guiding in the case of more pulse energy is discussed in the supplementary file, here we only show the resulting energy spectrum in figure 7(c). The cut-off energy is much higher in this case, which is the consequence of beam-driven plasma wakefield acceleration, detailed in the next section. We also compare the angular distribution of accelerated electrons in figure 7(d), where the beam-driven (high-intensity) case provides the less divergent electron beam, but in all cases most of the electrons have a divergence less than 0.5° (9 mrad).

It is also important to see what would happen without the capillary stage, therefore an additional simulation has been performed, where the first and last stages are moved close to each other, as it is shown in figure 8(a). In this case the distance between the centers of the gas jets is 800 μm, which still allows a density down-ramp section, where electrons can be injected. Near the half way of the full distance ($x \approx 1$ mm) we observed strong reflection from the boundaries due to the large divergence of the laser pulse after entering the second gas jet. The evolution of the electron phase-space distribution is shown in figure 8(b). At later times the electron bunch probably gets decelerated in the self-generated wakefield, which is shown in the inset. On the other hand, the electron bunch enters the region of the plasma wave, where the longitudinal electric field is positive due to the shortening of the plasma wavelength. The energy spectrum corresponding to the to last point in figure 8 is shown in figure 7. The evolution of the laser field amplitude also suggests that re-focusing of the laser pulse does not occur in this case, because of three reasons: energy depletion, plasma dispersion and electron density modulation. Inside a capillary these effects are much weaker, due to the lower density, and the diffraction is compensated by the concave density profile.

One can estimate a simplified electron energy scaling by keeping the peak intensity and pulse duration the same, while increasing the laser spot size by factor of κ. In this case the pulse energy increases by factor of κ^2, but the plasma density has to be reduced by κ^2 following the condition $\lambda_p \propto w_0$. If we consider that the propagation distance is proportional to the Rayleigh-length in vacuum ($L_R \propto \kappa^2$), then the electrons energy scales linearly with κ, since the electric field scales as $E_x \propto \sqrt{n_e} \propto \kappa^{-1}$. Thus, doubling the spot size (four times higher pulse energy) would lead to two times higher electron energy, which means ≈0.9 GeV quasi mono-energetic electron bunch produced by a 0.88 J laser pulse.

4. Transition to the beam-driven plasma wakefield acceleration regime

By increasing the laser pulse energy the self injection of electrons becomes much more efficient, such that the injected charge is sufficient the modify the wakefield potential and to generate a secondary wakefield in the back side of the bubble. The density distribution in the capillary stage is shown in figure 9(a). The bubble driven by the electron bunch is much stronger than the one driven by the laser pulse. Later, when the plasma density is higher (in the second gas jet) and the pulse is focused again, the laser-driven bubble encircles the electron bunch, which now enhances the the accelerating field inside of the wake. This boosted acceleration happens in the second gas jet and leads to the large cut-off energy presented in figure 7(b).

In this regime we lose the control over the energy spread of the electron bunch. However, the laser guiding is more efficient (see supplementary material), since the radial laser intensity distribution is much narrower inside the capillary. On the other hand the setup can be also simplified, because the dephasing compensation is ineffective due to the beam loading, thus the density of the second gas jet can be flattop (or super-Gaussian), without tilting.

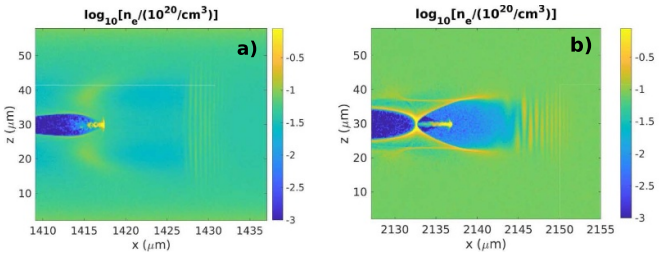

Figure 9. Density distribution of plasma electrons inside the capillary (a) and inside the second gas jet (b). In the simulation, where 20 % higher pulse energy is used.

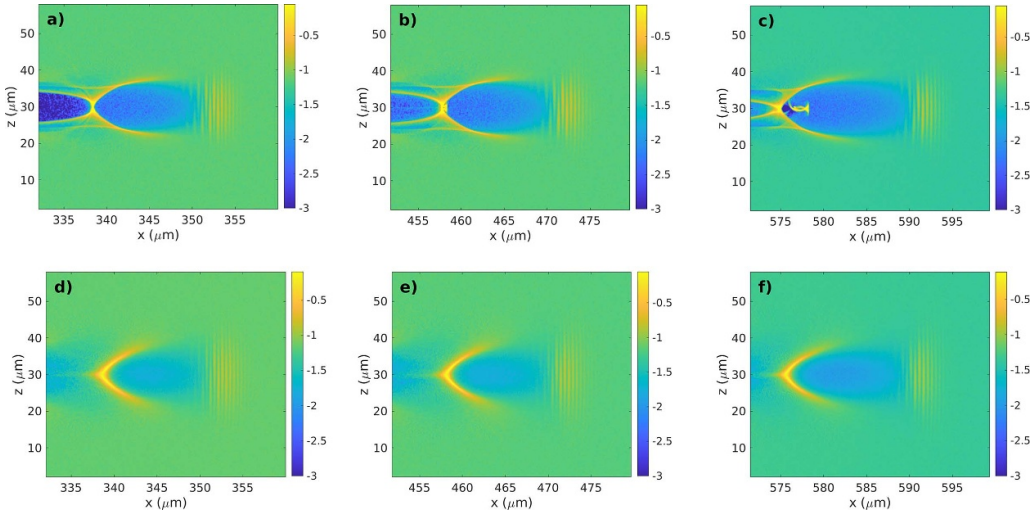

Figure 10. Density distribution of plasma electrons for two focus positions: $x_f = 250\,\mu$m (a)–(c) and $x_f = 50\,\mu$m (d)–(f).

5. Sensitivity of the scheme on different parameters

In this section the validity of the model's prediction is tested further, by performing additional simulations with mismatched parameters, used in figure 3. First, the effect of the focus position is emphasized in figure 10. The result agrees well with the expected scenario: if the laser pulse is focused too deep in the gas jet (figures 10(a)–(c)), then strong self focusing takes place and large charge is injected. The evolution of the transverse laser intensity is presented in the supplementary material, which shows that later inside the capillary the laser spot becomes much larger compared to the case with $x_f = 150\,\mu$m, which is the reference case. When the focus position is far outside of the gas jet (figures 10(d)–(f)), then self focusing and self injection does not occur. In this case ionization injection could be applied in the first gas jet, by mixing hydrogen with nitrogen, but the safe guiding of the laser pulse in the capillary is not guaranteed.

The predictions of figure 3(b) were also tested for two cases, which are presented in the supplementary material. The simulation result agrees well with the prediction of the modeling: when the capillary entrance is too far from the gas jet, the laser spot size increases drastically and the laser field interacts strongly with the capillary walls.

6. Conclusions

A yet unexplored regime of laser wakefield acceleration driven by few-cycle pulses has been studied numerically by using three-dimensional particle-in-cell simulations and by existing models for describing the evolution of the pulse envelope in the paraxial approximation. We found that the plasma non-uniformity in a Gaussian gas jet can alter the pulse propagation in a positive way, such that the pulse divergence remains small at the exit side of the gas jet. This feature is exploited to use a capillary for guiding, or re-focusing, the laser pulse which can post-accelerate the injected electrons in a second gas jet, which is tilted in order to compensate the de-phasing. The scheme presented here is best suited for laser pulses longer than $\approx$10 fs and wider than $\approx 10\,\mu$m. These parameters seem to be the absolute minimum requirements for the extension of the acceleration length by means of external guiding and for achieving good quality electron beams. In the case of shorter or more tightly focused pulses the plasma dispersion and radial diffraction are too strong.

For comparison we have presented a scenario, where the capillary stage is not present. This simulation shows the necessity of a guiding plasma channel, since the pulse gets easily diffracted in the second gas jet, where the density is much higher than in the capillary. Due to the lower density inside

the capillary the plasma dispersion and energy depletion are weak effects in this stage, and the radial compression of the laser pulse becomes possible. In addition, simulations were performed to test the sensitivity of the three-stage scheme on mismatched setups, which can easily happen in experiments and significantly alter the outgoing electron bunch quality.

Finally, a comparison has been made with the setup presented in [12], where basically the first two stages of our scheme were included. Although in our setup the pulse energy six times lower, we obtained similar central energies (≈300 MeV) for the electron bunches, which can be explained by the careful choice of plasma density inside the capillary. In our setup the plasma wavelength is matched to the electrons location relative to the driver pulse. Another important difference is that the laser focus position is placed in front of the gas jet, not behind it, as in [12], therefore the capillary guiding is more critical in our case. In this work we have proven that the laser pulse energy can be exploited more efficiently by adding a second gas jet, that serves as an energy booster and de-chirper, providing high quality electron bunches with higher energy. The energy cutoff can be almost doubled if the pulse energy is increased only by 20 %, leading to GeV-scale electron accelerator by using less than half Joule laser energy.

Data availability statement

The data cannot be made publicly available upon publication because no suitable repository exists for hosting data in this field of study. The data that support the findings of this study are available upon reasonable request from the authors.

Acknowledgments

We acknowledge KIFÜ/NIIF for awarding us access to HPC resource based in Debrecen, Hungary. The authors gratefully acknowledge the Gauss Centre for Supercomputing e.V. (www.gauss-centre.eu) for funding this project by providing computing time through the John von Neumann Institute for Computing (NIC) on the GCS Supercomputer JUWELS [44] at Jülich Supercomputing Centre (JSC). The ELI-ALPS Project (GINOP-2.3.6-15-2015-00001) is supported by the European Union and co-financed by the European Regional Development Fund. This work is partially supported by National Research, Development and Innovation Fund of Hungary (2020- 1.2.4-TÉT-IPARI-2021-00018).

ORCID iDs

Zsolt Lécz https://orcid.org/0000-0001-5968-8012
Daniel Papp https://orcid.org/0000-0002-7954-3686

References

[1] Leemans W P, Nagler B, Gonsalves A J, Tóth C, Nakamura K, Geddes C G R, Esarey E, Schroeder C B and Hooker S M 2006 *Nat. Phys.* **2** 696
[2] Leemans W P *et al* 2014 *Phys. Rev. Lett.* **113** 245002
[3] Spence D J, Butler A and Hooker S M 2003 *J. Opt. Soc. Am.* B **20** 138
[4] Gonsalves A J *et al* 2019 *Phys. Rev. Lett.* **122** 0840801
[5] Decker C D, Mori W B, Tzeng K-C and Katsouleas T 1996 *Phys. Plasmas* **3** 2047
[6] Alejo A, Cowley J, Picksley A, Walczak R and Hooker S M 2022 *Phys. Rev. Accel. Beams* **25** 011301
[7] Wiggins S M, Reijnders M P, Abuazoum S, Hart K, Vieux G, Welsh G H, Issac R C, Yang X, Jones D R and Jaroszynski D A 2012 *J. Plasma Phys.* **78** 355
[8] Papp D, Necas A, Hafz N, Tajima T, Gales S, Mourou G, Szabo G and Kamperidis C 2022 *Photonics* **9** 826
[9] Audet T L *et al* 2021 *Phys. Rev. Accel. Beams* **24** 073402
[10] Polanek R, Hafz N A M, Lécz Z, Papp D, Kamperidis C, Brunner S, Szabó E R, Tőkés T and Hideghéty K 2021 *Nucl. Instrum. Methods Phys. Res.* A **987** 164841
[11] Papp D, Lécz Z, Kamperidis C and Hafz N A M 2021 *Plasma Phys. Control. Fusion* **63** 065019
[12] Gonsalves A J *et al* 2011 *Nat. Phys.* **7** 862
[13] Ke L T *et al* 2021 *Phys. Rev. Lett.* **126** 214801
[14] Schmid K *et al* 2009 *Phys. Rev. Lett.* **102** 124801
[15] Schmid K, Buck A, Sears C M S, Mikhailova J M, Tautz R, Herrmann D, Geissler M, Krausz F and Veisz L 2010 *Phys. Rev. ST Accel. Beams* **13** 091301
[16] Veisz L *et al* 2009 *C. R. Physique* **10** 140–7
[17] Alehi F S, Goers A J, Hine G A, Feder L, Kuk D, Miao B, Woodbury D, Kim K Y and Milchberg H M 2017 *Opt. Lett.* **42** 215
[18] Salehi F, Le M, Railing L, Kolesik M and Milchberg H M 2021 *Phys. Rev.* X **11** 021055
[19] Gonsalves A J *et al* 2016 *J. Appl. Phys.* **119** 033302
[20] D'Arcy R *et al* 2022 *Nature* **603** 58–62
[21] Sprangle P, Esarey E and Ting A 1990 *Phys. Rev.* A **41** 4463
[22] Sprangle P, Esarey E, Krall J and Joyce G 1992 *Phys. Rev. Lett.* **69** 2200
[23] Sprangle P, Hafizi B, Peñano J R, Hubbard R F, Ting A, Zigler A and Antonsen T M 2000 *Phys. Rev. Lett.* **85** 5110
[24] Esarey E, Sprangle P, Krall J, Ting A and Joyce G 1993 *Phys. Fluids* B **5** 2690
[25] Esarey E, Krall J and Sprangle P 1994 *Phys. Rev. Lett.* **72** 2887
[26] Yazdanpanah J 2019 *Plasma Phys. Control. Fusion* **61** 085021
[27] Thomas A G R *et al* 2007 *Phys. Rev. Lett.* **98** 095004
[28] Ralph J E, Marsh K A, Pak A E, Lu W, Clayton C E, Fang F, Mori W B and Joshi C 2009 *Phys. Rev. Lett.* **102** 175003
[29] Poder K *et al* 2018 *Plasma Phys. Control. Fusion* **60** 014022
[30] Sprangle P, Tang C-M and Esarey E 1987 *IEEE Trans. Plasma Sci.* **15** 145
[31] Lu W, Tzoufras M, Joshi C, Tsung F S, Mori W B, Vieira J, Fonseca R A and Silva L O 2007 *Phys. Rev. ST Accel. Beams* **10** 061301
[32] Arber T D *et al* 2015 *Plasma Phys. Control. Fusion* **57** 113001
[33] Esarey E, Sprangle P, Krall J and Ting A 1997 *IEEE J. Quantum Electron.* **33** 1879
[34] Bobrova N A, Esaulov A A, Sakai J-I, Sasorov P V, Spence D J, Butler A, Hooker S M and Bulanov S V 2001 *Phys. Rev.* E **65** 016407

[35] Bobrova N A, Bulanov S V, Esaulov A A and Sasorov P V 2000 *Plasma Phys. Rep.* **26** 10
[36] Shiraishi S *et al* 2013 *Phys. Plasmas* **20** 063103
[37] Feit M D, Komashko A M, Musher S L, Rubenchik A M and Turitsyn S K 1998 *Phys. Rev.* E **57** 7122
[38] Patil S D, Takale M V, Fulari V J, Gupta D N and Suk H 2013 *Appl. Phys.* B **111** 1–6
[39] Kovalev V F and Bychenkov V 2018 *JETP Lett.* **107** 458
[40] Esarey E and Leemans W P 1999 *Phys. Rev.* E **59** 1082
[41] Cormier-Michel E, Esarey E, Geddes C G R, Schroeder C B, Paul K, Mullowney P J, Cary J R and Leemans W P 2011 *Phys. Rev. ST Accel. Beams* **14** 031303
[42] Swanson K K *et al* 2021 *Phys. Rev. Accel. Beams* **24** 091301
[43] Guillaume E *et al* 2015 *Phys. Rev. Lett.* **115** 155002
[44] Alvarez D 2021 JUWELS cluster and booster: exascale pathfinder with modular supercomputing architecture at Juelich Supercomputing Centre *J. Large-Scale Res. Facil.* **7** A183